ResearchGate

See discussions, stats, and author profiles for this publication at: https://www.researchgate.net/publication/7071545

Infants with Perinatal Hypoxic Ischemia: Feasibility of Fiber Tracking at Birth and 3 Months 1

Article *in* Radiology · August 2006

DOI: 10.1148/radiol.2393041523 · Source: PubMed

CITATIONS
19

READS
28

5 authors, including:

Carola van Pul
Maxima Medical Center
39 PUBLICATIONS **371** CITATIONS
SEE PROFILE

Jan Buijs
Maxima Medical Center
12 PUBLICATIONS **147** CITATIONS
SEE PROFILE

Anna Vilanova
Delft University of Technology
141 PUBLICATIONS **1,353** CITATIONS
SEE PROFILE

P.F.F. Wijn
Maxima Medical Center
93 PUBLICATIONS **1,044** CITATIONS
SEE PROFILE

Some of the authors of this publication are also working on these related projects:

High-Dimensional Single-Cell Analysis By Mass Cytometry (CyTOF) Of The Mucosal Intestinal Immune System In Health And Disease. View project

All content following this page was uploaded by Carola van Pul on 30 September 2014.

The user has requested enhancement of the downloaded file. All in-text references underlined in blue are added to the original document and are linked to publications on ResearchGate, letting you access and read them immediately.

Infants with Perinatal Hypoxic Ischemia: Feasibility of Fiber Tracking at Birth and 3 Months[1]

Carola van Pul, PhD
Jan Buijs, MD
Anna Vilanova, PhD
F. George Roos, MD
Pieter F. F. Wijn, PhD

The purpose of this study was to retrospectively investigate the feasibility of fiber tracking at birth and 3 months in infants with hypoxic ischemia to detect disturbances in white matter development. This retrospective study did not require institutional review board approval. All parents gave informed consent. Diffusion-tensor magnetic resonance (MR) images were obtained in full-term newborns: seven with standard MR imaging findings and 10 with perinatal hypoxic ischemia–related abnormalities. Visualization of white matter tracts was investigated by using a volume-tracing and quantification technique. Fiber tracking was useful for studying the neonatal brain. Abnormalities resulted in fiber patterns that were different from the fiber patterns of normal brain tissue. The corona radiata fibers were frequently affected.

© RSNA, 2006

[1] From the Departments of Clinical Physics (C.v.P., P.F.F.W.), Neonatology (J.B.), and Radiology (F.G.R.), Máxima Medical Center Veldhoven, De Run 4600, PO Box 7777, 5500 MB Veldhoven, the Netherlands; and Departments of Applied Physics (C.v.P., P.F.F.W.) and Biomedical Engineering (A.V.), Eindhoven University of Technology, Eindhoven, the Netherlands. Received September 3, 2004; revision requested November 11; revision received February 3, 2005; accepted March 11; final version accepted August 1. **Address correspondence to** C.v.P. (e-mail: *C.vanPul@mmc.nl*).

© RSNA, 2006

Cerebral white matter myelination is known to start in utero and to continue during the first year of life (1). At birth, myelination is observed in only a few cerebral white matter structures; among these are the posterior limb of the internal capsule (PLIC) and the central part of the corona radiata (CR). During the first months of life, the optic radiation and the splenium of the corpus callosum (CC) become myelinated; the anterior limb of the internal capsule and the genu of the CC become myelinated at 3–6 months (1–3).

The process of myelination can be followed by using conventional magnetic resonance (MR) imaging techniques, such as T1- and T2-weighted imaging (4), or by using the relatively recently introduced technique, diffusion-tensor imaging (5–7). A preference of water molecules for diffusion in a particular direction (ie, anisotropic diffusion) reflects the underlying tissue structure. Diffusion-tensor imaging is based on the acquisition of a tensor to describe diffusion. The main eigenvector of the diffusion tensor defines the preferred direction when the underlying tissue structure (eg, white matter) is linear (8,9). Various methods for visualization of the diffusion anisotropy and the preferred direction are available and include anisotropy maps that display the anisotropy index (10) and color maps that depict the diffusion direction with color-coded pixels (11–13). Fiber tracking, a relatively recently introduced technology, is a three-dimensional visualization technique in which the underlying linear structure defined by the diffusion tensor is reconstructed (9,14–16).

White matter in the adult brain is highly myelinated, and visualization of the main direction of diffusion corresponds to known white matter pathways on anatomy atlases, as outlined in detail on a recently published brain fiber atlas (13). In neonates, the white matter is still developing. Diffusion anisotropy has been reported to occur before myelination occurs and to increase with increasing myelination (5–7,17).

The preliminary results of fiber tracking with 3.0-T MR imaging in newborns obtained by Zhai et al (18) show that this technique is feasible in the neonatal brain, although only the major white matter tracts could be traced. In a case report of one neonate and two children aged approximately 2 years, fiber tracking was shown to yield additional information about the white matter configuration during dysgenesis of the CC (19). Furthermore, asymmetry in the pyramidal tracts has been observed in children with congenital hemiparesis (20).

A high incidence of severe motor problems in newborns with hypoxic-ischemic injury in the white matter and/or injury in the basal ganglia has been reported (1,21,22). Thus, the purpose of our study was to retrospectively investigate the feasibility of fiber tracking at birth and 3 months in infants with hypoxic ischemia to detect disturbances in white matter development.

Materials and Methods

At our medical center (Máxima Medical Center Veldhoven), an MR imaging protocol, including diffusion-tensor imaging, has been approved by the board of the neonatal department to be part of our normal clinical routine. All parents gave informed consent for the inclusion of their babies' imaging and clinical data in this study. We consulted our institutional review board, which did not require its approval for this retrospective study. All infants with abnormalities observed on MR images obtained during the first month after the onset of symptoms were reexamined at ages 3–4 months for determination of either the final extent of the possible injury or normal brain development. We retrospectively selected all neonatal patients in whom diffusion-tensor images that were suitable for fiber tracking had been obtained.

Infant Patient Group

The study group was recruited from a group of neonates who were born at term with perinatal hypoxic ischemia and were treated in our neonatal intensive care unit. Perinatal hypoxic ischemia was diagnosed when clinical symptoms of neonatal encephalopathy were present with two or more of the following risk factors during the first days of life: fetal heart rate abnormality, umbilical artery pH level lower than 7.10, meconium-stained fluid, and Apgar score 5 minutes after birth lower than 7. Included in our study group were all infants from this group in whom a diffusion-tensor image suitable for fiber tracking at birth and at 3 months was obtained. All babies with congenital abnormalities, neurometabolic disease, and/or perinatal infection were excluded.

The data from a total of 10 full-term infants were included between November 2002 and June 2004. All included babies were born after an uneventful pregnancy. The onset of symptoms could be timed to the day of birth. The newborns (nine male, one female) had a mean gestational age of 40.2 weeks ± 1.6 (standard deviation σ in the group) and were imaged at ages 1–9 days (n = 9); one baby was imaged 17 days after birth. Follow-up MR imaging was performed a mean of 3.4 months ± 0.5 later. Neurodevelopmental evaluations were performed when the infants were between 6 and 12 months of age, according to the protocol of Amiel-Tison et al (23). The Bayley Scales of Infant

Published online before print
10.1148/radiol.2393041523

Radiology 2006; 240:203–214

Abbreviations:
ADC = apparent diffusion coefficient
CC = corpus callosum
CI = linear anisotropy index
CR = corona radiata
IFO/OR = inferior fronto-occipital fasciculus and/or optic radiation
PLIC = posterior limb of internal capsule
ROI = region of interest

Author contributions:
Guarantor of integrity of entire study, P.F.F.W.; study concepts/study design or data acquisition or data analysis/interpretation, all authors; manuscript drafting or manuscript revision for important intellectual content, all authors; manuscript final version approval, all authors; literature research, C.v.P., J.B., A.V.; clinical studies, C.v.P., J.B., A.V., F.G.R.; statistical analysis, C.v.P., P.F.F.W.; and manuscript editing, C.v.P., J.B., A.V.

Authors stated no financial relationship to disclose.

Development (edition 2, Dutch version) were used to test the psychomotor development of the infants when they were aged 1 year or older. According to the Bayley classification system, a psychomotor development score lower than -2σ indicates severe delay and a score between -2σ and -1σ indicates moderate delay. Neurodevelopmental examinations were performed in the infants at ages 6 months ($n = 5$) and 1 year ($n = 5$).

Reference Values

Because we did not have a control group of healthy newborns, we obtained reference values from seven full-term newborns in whom MR imaging was performed for clinical purposes during the same period that the newborns in the patient group were imaged. The reference values were obtained from full-term newborns who had various clinical symptoms; the values were not chosen by using the criteria used to select the hypoxic-ischemic encephalopathy group. The newborns in this reference group had clinical symptoms of Sarnat stage 1 or 2 perinatal hypoxic ischemia (five babies), perinatal infection (one baby), and mild persistent neonatal pulmonary hypertension (one baby, who needed endotracheal ventilation for 3 days and nitric oxide therapy for 1 day and had a normal clinical short- and long-term follow-up). All of these newborns were imaged 4–13 days after birth. MR imaging revealed normal findings ($n = 4$), minor signal intensity abnormalities in the cortex (ie, high signal intensity on the T1-weighted image [22]) with no signal intensity abnormalities in the white matter ($n = 2$), or a minor abnormality in the cerebellum ($n = 1$). This reference group consisted of one female and six male neonates with a mean gestational age of 39.0 weeks ± 1.6. Their brain development and myelination were assessed at T1- and T2-weighted imaging and found to be normal. It was verified that no abnormalities were visible on the diffusion-weighted images, all of which were acquired within the first week after birth (by J.B., F.G.R.). The same neurodevelopmental examinations that were performed in the patient group were performed in these children at ages 6 months (two babies) and 1 year (five babies). All of these babies were deemed to be developmentally healthy. Two babies in this group were examined at follow-up MR imaging, including diffusion-tensor imaging, at age 3½ months.

MR Imaging Protocol

A 1.0-T MR imaging unit (Gyroscan; Philips Medical Systems, Best, the Netherlands) was used. The imaging protocol included the acquisition of T1-weighted spin-echo (568/18 [repetition time msec/echo time msec]), T2-weighted fast spin-echo (4381/120), and inversion-recovery (3436/18/400 [repetition time msec/echo time msec/inversion time msec]) MR images. The neonatal patients were sedated with chloral hydrate and fixated by using a vacuum pillow. For all brain imaging, a standard birdcage head coil was used.

The imaging protocol also included diffusion-tensor imaging, which was performed by using pulsed field gradients in six directions with single-shot echo-planar MR imaging. In the neonatal brain, 20 adjacent sections were recorded within 3 minutes with 3595/82 and a voxel size of $1.56 \times 1.56 \times 3$ mm. Two signals were acquired. Three b values (0, 400, and 800 sec/mm^2) were used to calculate the apparent diffusion coefficient (ADC). A duration of one gradient lobe of the pulsed field gradients of 20.06 msec, a time between the onset of the first gradient lobe and the onset of the second gradient lobe of 40.5 msec, and a gradient lobe strength of 19.6 mT/m were used with a b of 400 sec/mm^2, and a gradient lobe strength of 27.8 mT/m (by combining the x, y, and z gradients) was used with a b of 800 sec/mm^2. We chose to use b values lower than those used in the adult brain (typically 1000 sec/mm^2) because the ADC in the white matter of neonates is higher than that in the white matter of adults. The optimal b value was calculated by using the method of Jones et al (24).

Postprocessing and Image Analysis

ADC maps were constructed by using software on the MR imaging unit. The diffusion-tensor images were converted into the file format used in the fiber-tracking program by using Mathematica 4.2 software (Wolfram Research, Urbana, Ill). For display of global information, color mapping and fiber tracking were implemented. Color mapping was performed by mapping the first eigenvector of the diffusion tensor directly to the red-green-blue channel and thereby color coding the diffusion direction. Fiber tracking is based on the line propagation technique (9), which involves the use of the second-order Runge-Kutta method for numerical integration. Stopping criteria, which are used in the fiber-tracking procedure to determine when the tracking is to be stopped, could be defined by the user. Examples of user-defined stopping criteria would be an anisotropy value smaller than the threshold value and an α angle (maximal angle between connected vectors during fiber tracking) larger than the threshold angle. For visualization, the user could also choose to display only fibers of a certain length. The stopping criteria that were used in this study are listed in Table 1.

A problem with fiber tracking is that of selecting the seed points from which the fiber tracking will be started. Usually, the seed points are defined by the user—for example, by defining an ROI, which requires prior knowledge about the structures in the data set. The disadvantage of using this seed point selection method is that information can be easily missed when abnormalities are present in the data set. For example, when fibers are disrupted, ROI-based tracing will be stopped in the disrupted area, and the other part of the fiber—if it is intact—will not be detected. Furthermore, the fact that it is unknown which tracts in the brain of a newborn can be visualized complicates fiber tracking.

We have implemented a volume-tracing method of fiber tracking in which all voxels are considered as possible seed points. This approach yields long and evenly spaced fibers. The user defines how dense the visualized fibers must be by choosing values for the minimal distance between the seed points and the fibers and for the minimal dis-

tance allowed between the fibers once tracking has started. Tracking of a given fiber stops if the tracking starts to occur too close to other fibers—that is, within a distance that is less than the minimal distance allowed between the fibers during tracking. This algorithm has been described in detail previously (25).

For detailed visualization of a particular white matter structure, multiple ROIs for seed point selection can be defined. ROIs that are sampled uniformly to generate seed points are called "Or ROIs" derived by using the "Or" criterion. ROIs defined to show the fibers that pass through it are called "And ROIs" derived by using the "And" criterion. If no ROI derived with the "Or" criterion is defined, then the entire volume is seeded and just the fibers that pass through the "And" ROI are shown. This method prevents structures from being missed owing to undersampling of the ROI. It must be noted that, in contrast to conventionally displayed radiologic images, fiber-tracking images cannot always be displayed from the feet to the head. Therefore, for all images, the viewpoint has been indicated.

The color maps were used to evaluate the directionality and anisotropy of several white matter structures by means of visual inspection. The structural information observed on the color maps was compared with the structures observed on the color maps used by Makris et al (11), Wakana et al (13), and Jellison et al (26). Quantitative anisotropy maps were used to determine whether anisotropy was increased in affected regions and thus to determine whether this increased anisotropy could influence the fiber tracking. Volume tracing was used to determine, in a user-independent way, which fiber structures were visible. The obtained fiber-tracking images were compared with the fiber-tracking atlases defined by Wakana et al (13) and Jellison et al (26). The color maps, anisotropy maps, and fiber-tracking images were evaluated and interpreted in consensus by three authors (C.v.P., J.B., and F.G.R., all with 5 years experience in pediatric brain MR imaging and/or diffusion-tensor imaging). The fiber structures observed in the babies with standard MR imaging findings served as a reference.

The fiber structures observed in the babies at 3 months were compared with the structures observed in the same babies at birth. Some tracts, like the inferior fronto-occipital fasciculus and the optic radiation, have been reported to course close together and to be oriented in a similar direction (26–28). These tracts could not be detected separately by using color mapping or volume tracing and were therefore considered to be a combined tract (ie, fronto-occipital fasciculus and/or optic radiation [IFO/OR] tract); thus, "IFO/OR" indicated that the fiber path detected could have corresponded to either or both tracts. These tracts can be separated by using ROIs with the "And" criterion; however, this process was not performed in this study. We used the term *fiber pathology* to describe an abnormality in which a visible asymmetry in the fiber pattern between the left and right hemispheres or a large deviation in the fiber pattern, as compared with the fiber pattern in the reference infant group, was observed. After determining which structures were visible, with use of an ROI-based tracing method, we defined multiple ROIs to visualize the structures observed at volume tracing in more detail.

We chose the anisotropy index Cl—not fractional anisotropy or relative anisotropy—as a stopping criterion because it is more sensitive to linear anisotropy and less sensitive to planar anisotropy, as determined by using normalized eigenvalue space plots (29). The values for Cl were based on the values measured in neonatal white matter and CC (30). To avoid fiber information cluttering, the chosen value at which fiber volume tracing was stopped was larger than that at which ROI-based tracing was stopped (Table 1).

With both volume tracing and ROI-based tracing, fibers were displayed only if they were longer than a user-defined length, because visualization of the smaller fibers could have resulted in additional information cluttering. For neonates at birth, a minimal length of greater than 3 mm was used, and for babies at 3 months of age, a minimal length of greater than 5 mm was used (Table 1).

Table 1

Criteria Used to Stop Fiber Tracking in Patient Groups and Evaluation Methods

Patient Group	Criteria to Stop Volume Tracing	Criteria to Stop ROI-based Tracing	Criteria to Stop PLIC Fiber Measurements
Neonates at birth	$Cl < 0.12$	$Cl < 0.08$	$Cl < 0.12$
	$\alpha < 10°$	$\alpha < 10°$	$\alpha < 10°$
	$L > 3$ mm	$L > 3$ mm	$L > 0$ mm
Infants aged 3 mo	$Cl < 0.14$	$Cl < 0.10$	$Cl < 0.12$
	$\alpha < 10°$	$\alpha < 10°$	$\alpha < 10°$
	$L > 5$ mm	$L > 5$ mm	$L > 0$ mm

Note.—With volume tracing, the minimal distance between the seed points and the fibers *(dl)* was 1.0 mm and the minimal distance allowed between the fibers was $0.5 \cdot dl$. The region-of-interest (ROI)-based method involved the use of four to six ROIs obtained with the "Or" criterion. To determine the length and volume of the PLIC fibers, two ROIs were drawn around the PLIC in two adjacent transversal sections and the "And" criterion was used. Different stopping criteria were used in babies at birth and in those aged 3 months, because the structures were more developed at 3 months and using the same stopping criteria could have led to information cluttering. With use of more stringent stopping criteria at 3 months, cluttering was prevented and no fiber information was lost. Cl = linear anisotropy index (ie, index sensitive to linear diffusion), L = length of the displayed fibers, α = maximal angle between connected vectors during fiber tracking.

Quantification of PLIC Fibers

The motor and somatosensory pathways in the CR pass perpendicular to the transversal plane through the PLIC (31). Herein, these fibers are referred to as PLIC fibers. To determine the length and volume of the PLIC fibers, two ROIs were drawn roughly around the PLIC in two adjacent transversal sections. We used the "And" criterion: Fiber tracking was initiated from all

points in the volume, and only those fibers passing through both ROIs were displayed. This technique was similar to the method used by Mori et al (31). If an abnormality was suspected to be disturbing fiber tracking, the pattern of disturbance was checked by using volume tracing. The detected disturbance pattern would be used to determine whether normal ROI selection should be used or the ROI selection should be defined in other nearby transversal sections to prevent fibers from being missed owing to ROI misplacement. Analysis of the PLIC fibers was performed in consensus by three authors (C.v.P., J.B., F.G.R.). After visualization of the PLIC fibers, the mean length of all the fibers was calculated. It must be noted that not the true length of the white matter fibers, but rather an indication of the length of the linear diffusion path of diffusing water molecules, was determined. The fiber volume was the volume of all pixels through which one or more fibers passed. In all infants, the mean fiber lengths and volumes calculated with three CI values (0.08, 0.10, and 0.12) were determined at birth and at 3 months.

Statistical Analyses

To compare the PLIC fiber lengths measured in the left and right hemispheres, a Student *t* test was used. A paired Student *t* test was used to compare the PLIC fiber lengths measured in neonates at birth with those measured in the same babies at 3 months. $P < .05$ was considered to indicate significance (32). Statistical analyses were performed by using Mathematica 4.2 software. These analyses were performed by two authors (C.v.P., P.F.F.W.).

Results

Color Maps

In the seven infants with standard MR imaging findings (reference group), the structures that were visible on the color maps at birth were evaluated. In this group, the following structures were clearly visible at birth: the PLIC in all seven infants; the anterior limb of the internal capsule in six; the posterior, middle, and frontal regions of the IFO/OR in all seven infants, six infants, and one infant, respectively; the fornix in six; the cingulum (directly above the CC) in six; and the superior region of the CR in all seven. Two infants in the reference group were examined with MR imaging at 3 months. A clear difference between the color maps obtained at

Figure 1

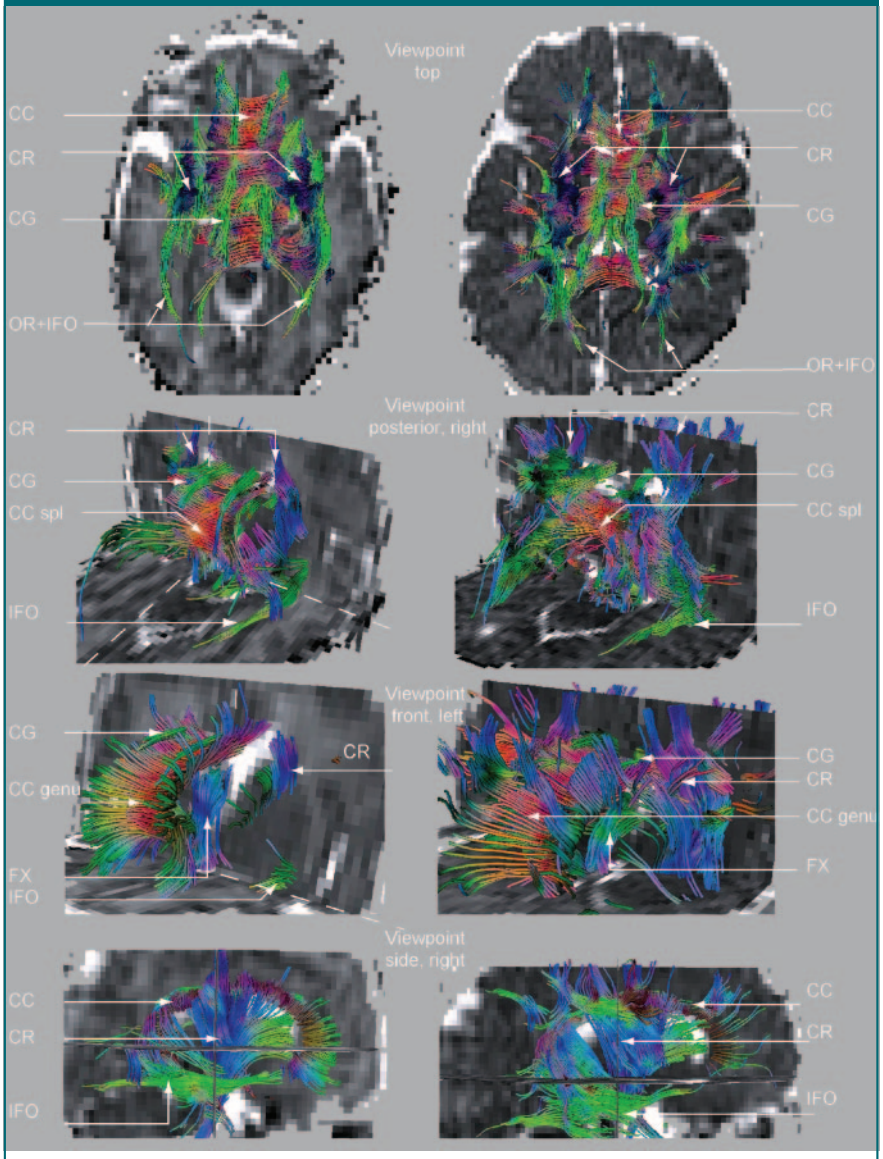

Figure 1: Left: Fiber-tracking images obtained at various angles in full-term newborn with standard MR imaging findings 6 days after birth. Right: Corresponding fiber-tracking images obtained in the same infant at 3 months. These three-dimensional fiber-tracking images are superimposed on two-dimensional ADC maps, which were constructed by using diffusion-tensor images acquired with pulsed field gradients in six directions with single-shot echo-planar MR imaging (3595/82, two signals acquired, 1.56 × 1.56 × 3-mm voxel size, *b* values of 0, 400, and 800 sec/mm^2). The main white matter structures are shown and closely match structures on the fiber-tracking atlas introduced by Wakana et al (13). The stopping criteria for ROI-based tracing summarized in Table 1 were used. *CG* = cingulum, *FX* = fornix, *spl* = splenium.

birth and those obtained at 3 months in these babies was observed. The anterior and posterior regions of the CR, as well as the superior fronto-occipital fasciculus and the superior longitudinal fasciculus, were visualized better at 3 months. Also, the IFO/OR, CC, and cingulum were more apparent. Most structures were less pronounced compared with the same structures in adults observed on the color maps described in several studies (11,13,26).

In the infant group with fiber abnormalities, the color maps showed a disturbed pattern compared with the fiber pattern observed in the reference infant group. In the affected areas, there was increased anisotropy, which was apparent in white matter areas and in the gyri.

Table 2

Abnormalities and Outcomes in Infant Patients

Patient No.	Main Abnormality at Birth	Fiber Abnormality at Birth	Main Abnormality at 3 mo	Fiber Abnormality at 3 mo	Outcome
1	Multifocal WM lesions, anisotropy strongly higher in R than in L hemisphere	None remarkable	Mildly delayed myelination, anisotropy nearly equal in R and L hemispheres	None remarkable	Normal findings at 6 mo
2	Multifocal WM lesions, anisotropy strongly higher in R than in L hemisphere	Anisotropy lower in R than in L CR	Local tissue loss, anisotropy strongly higher in R than in L hemisphere	None remarkable	Normal findings at 1 y
3	Multifocal WM lesions, anisotropy nearly equal in R and L hemispheres	Anisotropy strongly lower in R than in L IFO/OR	Normal MR findings	None remarkable	Normal findings at 1 y
4	Bilateral basal ganglia injury, anisotropy nearly equal in R and L hemispheres	Anisotropy in CR strongly lower than normal, anisotropy lower in R than in L IFO/OR	Low myelination in ALIC, anisotropy nearly equal in R and L parts of splenium of CC	Anisotropy lower in R than in L CR	Moderate neuromotor delay at 1 y
5	Minor basal ganglia injury, edema in R splenium of CC	Anisotropy strongly lower in R than in L splenium of CC and lower in L than in R IFO/OR	Delayed myelination in ALIC, anisotropy nearly equal in R and L hemispheres	Anisotropy lower in L than in R IFO/OR	Normal findings at 6 mo
6	Bilateral basal ganglia injury, diffuse WM injury, anisotropy nearly equal in R and L hemispheres	Anisotropy low, no fibers visible	WM and basal ganglia atrophy, anisotropy nearly equal in R and L hemispheres	Anisotropy in CR strongly lower than normal; CC, CG, and fornix not visible	Severe psychomotor retardation at 6 mo, death
7	Large infarct in territory of MCA and basal ganglia injury, all in L hemisphere	Anisotropy strongly lower in L than in R CR, splenium of CC, and IFO/OR	Severe tissue loss in infarct in L hemisphere	Anisotropy strongly lower in L than in R CR and IFO/OR, splenium of CC and cingulum not visible	R hemiplegia at 1 y
8	Large infarct and basal ganglia injury in L hemisphere	Anisotropy strongly lower in L than in R CR, strongly higher in L than in R splenium of CC, and strongly lower in L than in R IFO/OR*	Severe tissue loss in L hemisphere infarct	Anisotropy strongly lower in L than in R CR, lower in L than in R splenium of CC, and strongly lower in L than in R IFO/OR	R hemiplegia at 1 y
9	Occipital infarct affecting splenium of CC in L hemisphere	Anisotropy strongly higher in L than in R splenium of CC, strongly lower in L than in R IFO/OR*	Delayed myelination in internal capsule, anisotropy nearly equal in R and L hemispheres	Anisotropy strongly lower in R than in L splenium of CC	Hypertonia of arms and legs at 6 mo
10	Mild WM delay	None remarkable	Widened ventricles	None remarkable	Normal findings at 6 mo

Note.—ALIC = anterior limb of internal capsule, CG = cingulum, L = left, MCA = middle cerebral artery, R = right, WM = white matter.

* There was prolongation of splenium of CC tract owing to high anisotropy.

Fiber Tracking

In the infants with standard MR imaging findings, several white matter tracts could be appreciated on fiber-tracking images at birth and at 3 months (Fig 1). No differences between the right and left hemispheres were observed in this group. The following main white matter structures could be visualized with fiber tracking in these infants at birth: the CR in all seven babies, the genu and splenium of the CC in all seven; the entire CC in two; the posterior, middle, and frontal regions of the IFO/OR in all seven, six, and two babies, respectively; the fornix in all seven; and the cingulum (directly above the CC) in five. All other fibers defined on published fiber-tracking atlases (13,26) could not yet be detected at birth. It must be noted that in some newborns in the reference group, structures that were not well visualized on the color maps were visible on the fiber-tracking images. On the other hand, not all structures that were visible on the color maps were traceable at birth—for example, usually only a small part of the cingulum could be traced. In the two infants with standard MR imaging results available at 3 months, the structures observed at birth were more developed at 3 months, although newly developed structures could not be detected.

In the infants with abnormalities related to perinatal hypoxic ischemia, deviations in the expected pattern of fibers were observed in the regions of the abnormalities. A detailed overview of these findings is given in Table 2; the patients are grouped according to abnormality. In the patient group of 10 infants, the following fiber structures were frequently affected at birth: the CR in five babies, the IFO/OR in seven, and the CC in five. When these infants were aged 3 months, disturbed fiber patterns were still visible in the CR in four of them, in the IFO/OR in three, and in the CC in four. All of the infants who had disturbed patterns in the CR at 3 months demonstrated major motor problems.

Figure 2 shows examples of fiber tracking at birth and at 3 months in two infants with perinatal hypoxic ischemia–related abnormalities (patients 8 and 9 [Table 2]). Both infants had an infarct in the left hemisphere, but in patient 8 a larger area was affected. In patient 8, fibers were not traced in the CR (blue) at birth owing to the large infarct, which affected the basal ganglia also (Fig 2, top left). In the infarcted region, the anisotropy was inhomogeneously increased, and, thus, some fibers were

Figure 2

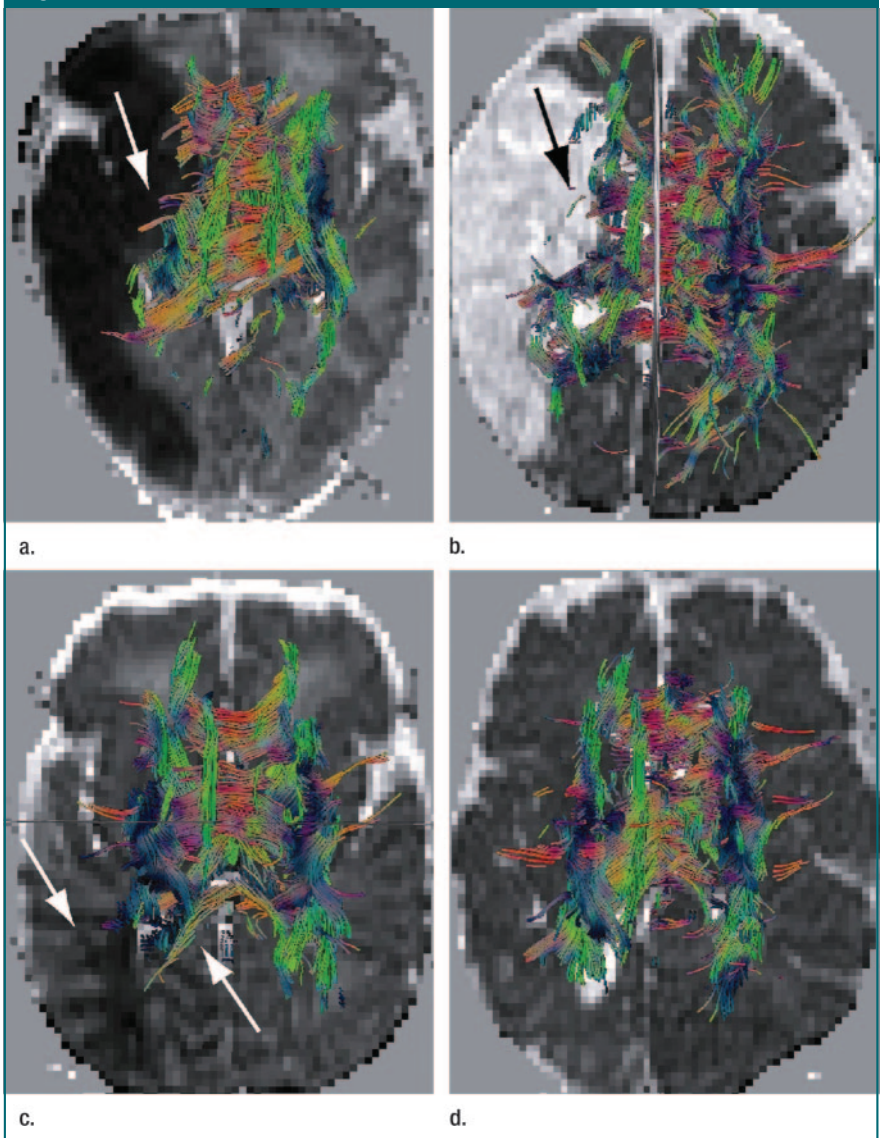

Figure 2: Fiber-tracking images obtained in **(a)** a newborn (patient 8, Table 2) at term and **(b)** the same infant at 3 months. Arrow points to region in which the CR fibers cannot be traced. **(c)** Fiber-tracking image obtained in patient 9 (Table 2) at term. Left arrow (pointing downward) indicates the infarct, which has a low ADC. Right arrow (pointing upward) indicates the splenium of the CC in the affected hemisphere, in which the splenium fibers are longer than those in the nonaffected hemisphere—probably owing to the abnormality. **(d)** Fiber-tracking image obtained in the same infant (patient 9) at 3 months. The splenium can be traced better in the affected hemisphere than in the nonaffected hemisphere. All images shown are three-dimensional fiber-tracking images superimposed on two-dimensional ADC maps, which were constructed from diffusion-tensor images acquired by using pulsed field gradients in six directions with single-shot echo-planar MR imaging (3595/82, two signals acquired, 1.56 × 1.56 × 3-mm voxel size, *b* values of 0, 400, and 800 sec/mm^2).

traced in this area and were considered fiber artifacts. Also, it is apparent that the IFO/OR was not traced in the affected hemisphere. At 3 months, the CR and IFO/OR in this infant still were not traceable (Fig 2, top right).

In patient 9 at birth, the splenium of the CC had an area of low ADC and high anisotropy (Fig 2, bottom left). The anisotropy was more increased in the left part of the CC than in the right, and, thus, longer fibers were traced in the left part compared with the fibers traced in the right part. The IFO/OR was less visible in the affected hemisphere than in the nonaffected hemisphere. At 3 months, a widened ventricle was observed in the affected hemisphere in this infant. Development of the posterior forceps of the CC was more pronounced in the affected hemisphere than in the nonaffected hemisphere.

One of the problems with using volume tracing is that information cluttering can occur during the tracing owing to artifacts on the MR images (Fig 3a), which do not occur when the ROI-based tracing method is used (Fig 3b). The data set displayed in Figure 3 is one of our worst examples. In general, the artifacts appeared as less dense lines. They could be easily distinguished from real fibers because they occurred only at the air-tissue boundaries. With our fiber-tracking protocol, it is possible to rotate the structures, use thick or thin fibers, and "look through" the cluttering.

Quantification of PLIC Fibers

In the infants with standard MR imaging findings, no remarkable differences between the left and right hemispheres were observed (Fig 4, two top rows). In patient 8, however, a clear difference in PLIC fiber length and volume between the left and right hemispheres was observed (Fig 4, two bottom rows). Furthermore, the fiber structures observed in the nonaffected hemispheres appeared to be smaller than normal.

Figure 3

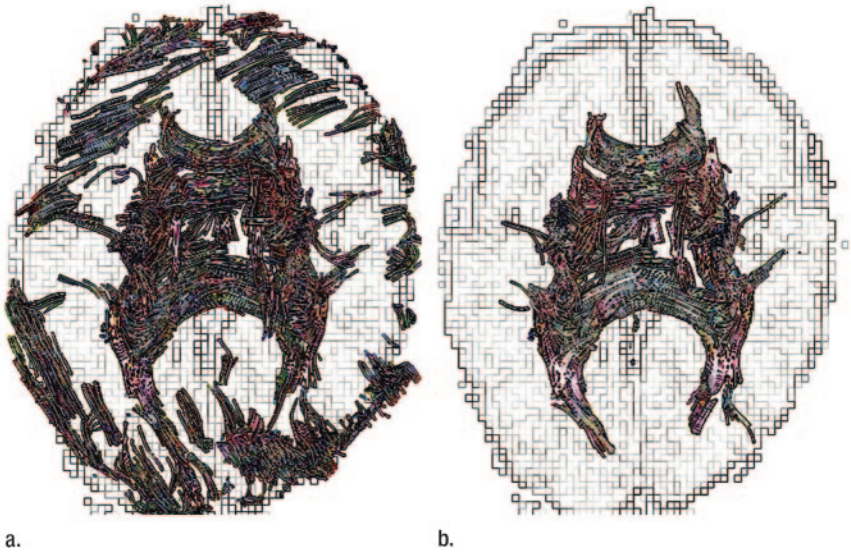

Figure 3: **(a)** Fiber-tracking image (top view) shows volume tracing in newborn with standard MR imaging findings. The typical artifacts that result from using single-shot diffusion-tensor echo-planar imaging are seen. **(b)** Fiber-tracking image (top view) obtained in the same infant by using five ROIs for seed point selection. Both of these three-dimensional fiber-tracking images are superimposed on two-dimensional ADC maps, which were converted by using edge detection to display the difference between fibers and background tissue more clearly. The ADC maps were calculated from diffusion-tensor images acquired by using pulsed field gradients in six directions with single-shot echo-planar MR imaging (3595/82, two signals acquired, $1.56 \times 1.56 \times 3$-mm voxel size, *b* values of 0, 400, and 800 sec/mm^2).

At Cl values of between 0.08 and 0.16, the fiber lengths in the infants with standard MR imaging findings were observed to have a linear dependency on the choice of the Cl as the stopping criterion. More important, the mean fiber lengths and volumes determined in the left and right hemispheres were comparable. Comparing values among these infants was possible as long as the same stopping criteria were used. At a Cl of 0.12, the mean PLIC fiber length in the reference infant group was 25 mm ± 4 (standard deviation σ in the group) for both hemispheres and the mean volume was 3.0 cm^3 ± 1.0 for both hemispheres.

Of the infants with fiber abnormalities, four had significantly reduced PLIC fiber lengths compared with the fiber lengths measured in the reference infant group (Fig 5a; values outside the shaded area indicate $P < .05$). In five patients, the measured fiber volumes were reduced significantly compared with the reference values ($P < .05$) (Fig 5b). The mean fiber length and volume in the patient group at 3 months were significantly increased compared with the values at birth ($P < .01$). For three infants (patients 6–8), the mean fiber volume (in one or both hemispheres) at 3 months deviated largely from the mean value for the other patients (Fig 5c, 5d). However, no comparable normal values were available because only two infants from the reference group were imaged at 3 months (Fig 5).

Discussion

Interpretation of Color Maps and Fiber-tracking Images

Color maps appear to be useful for determining whether the brain development in general is normal. However, interpretations of these images for the assessment of fiber structures are not straightforward. Fiber tracking is more suitable for these applications. However, because some parts of the inferior fronto-occipital fasciculus are close to the optic radiation (26–28), the separation of these tracts with volume tracing was not possible in our study. To visual-

ize white matter tracts in the neonatal brain, stopping criteria different from those used in the adult brain have to be used, because the anisotropy in the white matter of infants is lower.

Diffusion anisotropy has been observed before myelination occurred (5,6). Neil et al (5) divided the white matter regions visualized at birth into three types: *(a)* those packed into myelinated parallel bundles (type 1), *(b)* those with mostly nonmyelinated parallel bundles (type 2), and *(c)* those that are neither closely packed nor myelinated (type 3). Type 1 white matter tracts—for example, the central part of the CR that is myelinated in infants at birth—can be easily traced (2,6,33). The splenium of the CC and the optic radiation become myelinated in infants within the first 3 months and are type 2 tracts. These tracts can be visualized in infants at birth by using fiber tracking owing to the parallel orientation of the cell membranes. Type 3 white matter tracts cannot be visualized.

In the infants with fiber abnormalities, we observed disturbed fiber patterns. We must remark that when fibers are missed during fiber tracking, it does not mean that the white matter fibers are disconnected. This is, however, an indication that processes that have disturbed the diffusion have occurred.

It appears that the minor white matter abnormalities seen with fiber tracking (ie, asymmetry between hemispheres in a part of a traced fiber structure, the IFO/OR in particular) in our study tended to resolve at 3 months, while marked changes such as large fiber asymmetry persisted. All four patients who had large fiber abnormalities in the CR at 3 months had a poor outcome (ie, moderate to severe motor problems).

Several study investigators have reported that patients with hemiparesis have decreased anisotropy in the CR and the pyramidal tracts, which has been associated with loss of myelination and wallerian degeneration (20,34). In our study, the loss of fibers in the CR at birth was also visible at 3 months in four of the five patients in whom disturbed CR fibers were visible on the fiber-tracking images. In two of these infants, this fiber loss was associated with wallerian degeneration.

In a previous study, ischemia was observed to result in increased anisotropy in lesions in newborns (34). In two infants with ischemia in the splenium of the CC in our study, the increased anisotropy resulted in longer fibers being traced. The implications of these observations are not clear.

One of the limitations of our study was related to the criteria used to select the reference group. Although all of the infants in this group had standard MR imaging findings and normal short-term

Figure 4

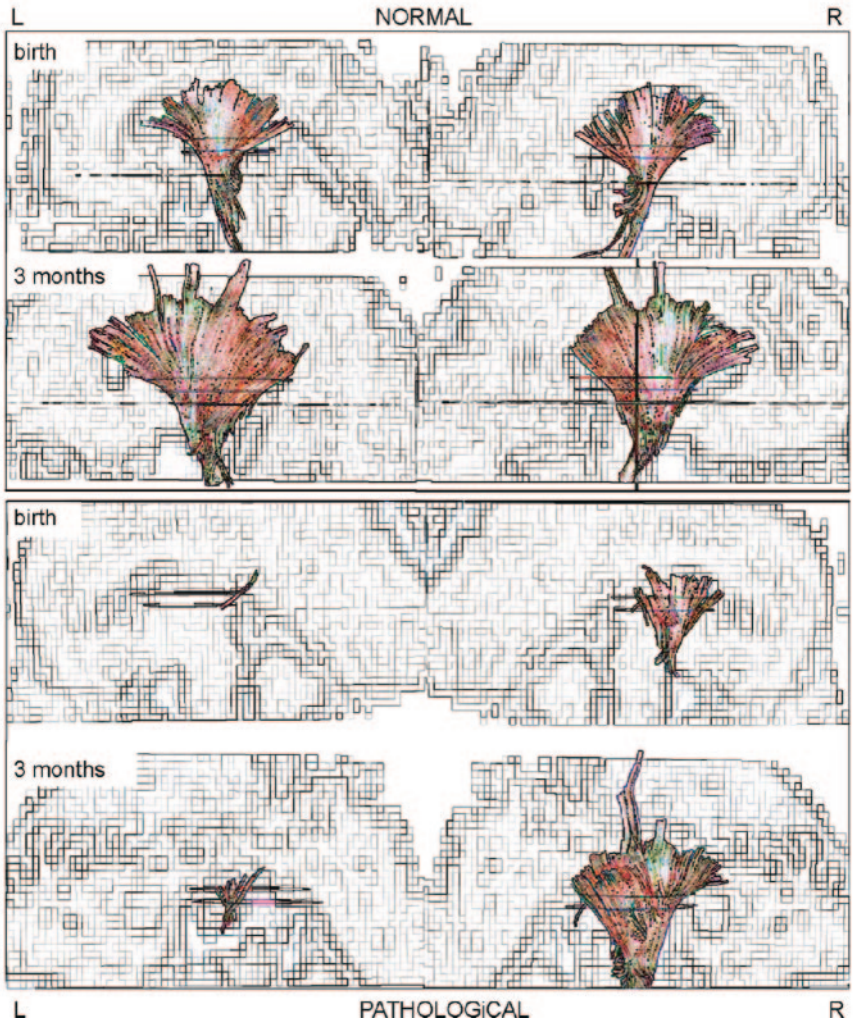

Figure 4: Traced fibers of the CR (viewpoint from the left in the left column and from the right in the right column). Top four images show fibers traced in an infant with standard MR imaging findings at birth and at 3 months. The difference in length and volume can be appreciated. Lower four images show fibers traced in an infant (patient 8) with fiber abnormality; asymmetry between the left and right hemispheres is immediately clear. The stopping criteria used for PLIC fiber tracking summarized in Table 1 were used. These three-dimensional fiber-tracking images are superimposed on two-dimensional ADC maps, which were converted by using edge detection to display the difference between fibers and background tissue more clearly. The ADC maps were constructed from diffusion-tensor images acquired by using pulsed field gradients in six directions with single-shot echo-planar MR imaging (3595/82, two signals acquired, 1.56 × 1.56 × 3-mm voxel size, *b* values of 0, 400, and 800 sec/mm^2).

follow-up results, we realize that the white matter in these babies could have been affected because they all were examined with MR imaging because of clinical indications. However, the general fiber pattern observed in these infants was similar, with no asymmetry; therefore, we assumed that this group could be used to obtain reference values.

Quantification of PLIC Fibers

Because the PLIC is myelinated at birth (2,6,20), ROI selection in this area results in a clear pattern of fibers, which include the motor and somatosensory tracts (31). Quantification of the lengths and volumes of PLIC fibers appears to be useful for detecting abnormalities, although the results must be carefully interpreted because they depend on the stopping criteria used. In most cases, the abnormality is directly visible owing to the asymmetry seen on the fiber-tracking images; however, in some patients the abnormality is less clear. Furthermore, quantification could be useful for identifying patients with global myelination delays in both hemispheres. The implications of detecting this type of abnormality for further neurologic development of the infant are not yet clear and require further study.

Fiber-tracking Methods and Study Limitations

Volume tracing enables user-independent fiber tracking. The advantages of using this method are that all fibers are traced and no fibers are missed as a result of ROI misplacement. Furthermore, if fibers appear to be disrupted, tracking from a single ROI will result in only part of the fibers being traced. In contrast, with use of volume tracing, all fibers, if present, will be detected as long as they display anisotropic diffusion. The main problem with the volume-tracing method is that typical diffusion-tensor and echo-planar imaging artifacts, such as image distortions due to eddy currents and air-tissue susceptibility effects, can result in erroneously large anisotropy values. The large anisotropy values result in what we call fiber artifacts, which can clutter the image. ROI-based tracing results in images with fewer artifacts, but it requires prior knowledge about the structures in the data set for correct ROI placement. By first using volume tracing to determine the presence of fiber structures and then performing ROI placement on the basis of the knowledge obtained with volume tracing, the best aspects of both techniques can be used.

One of the main limitations of all currently available fiber-tracking methods—this limitation was reported not only in our current study but also in other investigations (13)—is that the tracking is stopped in regions with planar anisotropy because no main direction of diffusion can be determined in these regions. With ROI-based tracing in particular, fibers might be missed owing to this limitation.

It must be noted that the fiber-tracking results reported herein should be carefully interpreted. First, the technique is not yet validated; however, in the myocardium, a good correlation between the direction of the first eigenvector and the histologic findings has been shown (35–37). In terms of white matter, good correspondence between the fiber-tracking results and the findings on anatomy atlases and/or in dissected anatomic sections has been observed (13,26,38).

Second, the fiber-tracking technique is susceptible to several errors, as extensively discussed in the articles of Basser et al (39), Tournier et al (40), and Mori and van Zijl (9). In our clinical practice, we use a 1.0-T MR system and relatively large voxels, in which partial volume effects occur. Furthermore, anisotropy is lower in the neonatal brain than in the adult brain. The inherently lower signal-to-noise ratio and lower anisotropy affect the accuracy of fiber

Figure 5

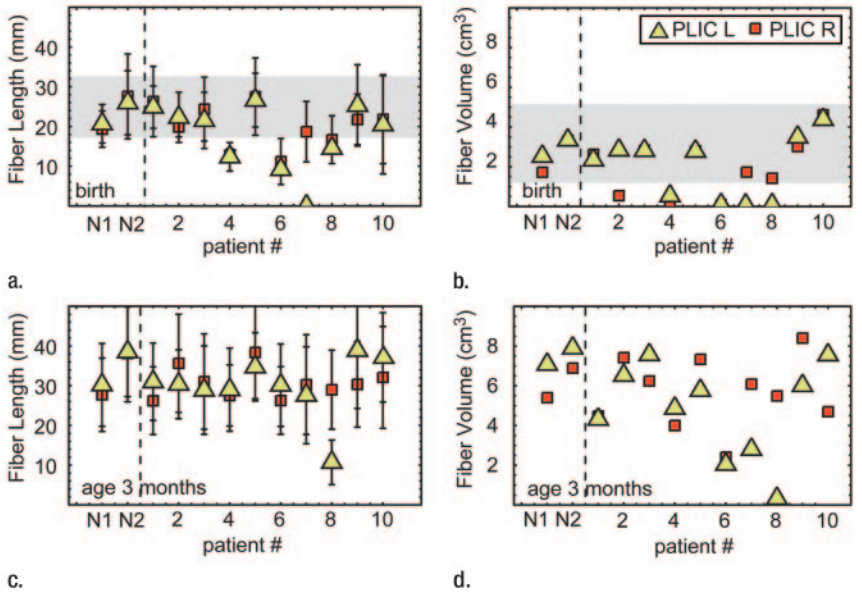

Figure 5: **(a, b)** Graphs show PLIC fiber lengths and volumes in two infants from the reference group (*N1* and *N2*) and the 10 infants from the patient group (abnormalities summarized in Table 2) at birth. Error bars indicate standard deviations of the mean fiber lengths. Shaded areas indicate 95% confidence intervals for values measured in the seven infants in the reference group. **(a)** The mean fiber length for four patients and **(b)** the mean fiber volume for five patients are outside the confidence intervals. The values in these patients were significantly ($P < .05$) different from normal. **(c, d)** Graphs show fiber lengths and volumes in the same two infants and 10 patients whose values are illustrated in **a** and **b**, at 3 months. The mean fiber lengths and volumes are greatly increased compared with the values at birth. **(d)** For three infants with abnormalities (patients 6–8), the mean fiber volume deviated largely from the other patients' values, in one or both hemispheres. In all four graphs, △ = left hemisphere, ■ = right hemisphere.

tracking. One problem that can occur owing to the low signal-to-noise ratio is tract jumping, in which the fiber path is determined erroneously (39). Furthermore, the anisotropy in a voxel can be obscured owing to partial volume effects. Tournier et al, by using simulations on synthetic data, showed that to identify small fibers, the signal-to-noise ratio needs to be high (40). This is probably the reason that we cannot distinguish small fiber tracts that are close to each other, like the fornix and the anterior commissure. Although several optimization steps still have to be taken, the main fiber tracts in the neonatal brain can be identified by using fiber tracking. Furthermore, the topologic features of the identified fibers correspond to expected white matter structures.

In conclusion, we have demonstrated the feasibility of fiber tracking—a user-independent volume-tracing method in particular—to study the neonatal brain. Abnormalities related to perinatal hypoxic ischemia resulted in fiber patterns that were different from the fiber structures detected in infants with standard MR imaging findings. Fiber tract abnormalities occurred frequently in the CR; this was expected because a high incidence of severe motor problems in asphyxiated newborns has been reported (1,21,22). With use of a quantification fiber-tracking method, an abnormality could be clearly seen as a difference between the hemispheres. Furthermore, significant differences in fiber lengths and volumes were observed between the infants with abnormalities in the basal ganglia and those with standard MR imaging findings. Further investigations are necessary to determine whether fiber abnormalities correlate with neonatal patient outcomes; our patient group was too small for us to make such conclusions.

References

1. Volpe JJ. Neurology of the newborn. 3rd ed. Philadelphia, Pa: Saunders, 1995.
2. Sie LT, van der Knaap MS, van Wezel-Meijler G, Valk J. MRI assessment of myelination of motor and sensory pathways in the brain of preterm and term-born infants. Neuropediatrics 1997;28:97–105.
3. Paus T, Collins DL, Evans AC, Leonard G, Pike B, Zijdenbos A. Maturation of white matter in the human brain: a review of magnetic resonance studies. Brain Res Bull 2001; 54:255–266.
4. van der Knaap MS, Valk J. MR imaging of the various stages of normal myelination during the first year of life. Neuroradiology 1990;31:459–470.
5. Neil JJ, Shiran SI, McKinstry RC, et al. Normal brain in human newborns: apparent diffusion coefficient and diffusion anisotropy measured by using diffusion tensor MR imaging. Radiology 1998;209:57–66.
6. Hüppi PS, Maier SE, Peled S, et al. Microstructural development of human newborn cerebral white matter assessed in vivo by diffusion tensor magnetic resonance imaging. Pediatr Res 1998;44:584–590.
7. Neil J, Miller J, Mukherjee P, Huppi PS. Diffusion tensor imaging of normal and injured developing human brain: a technical review. NMR Biomed 2002;15:543–552.
8. Basser PJ, Mattiello J, LeBihan D. Estimation of the effective self-diffusion tensor from the NMR spin echo. J Magn Reson B 1994; 103:247–254.
9. Mori S, van Zijl PC. Fiber tracking: principles and strategies. NMR Biomed 2002;15: 468–480.
10. Basser PJ, Pierpaoli C. Microstructural and physiological features of tissues elucidated by quantitative-diffusion-tensor MRI. J Magn Reson B 1996;111:209–219.
11. Makris N, Worth AJ, Sorensen AG, et al. Morphometry of in vivo human white matter association pathways with diffusion-weighted magnetic resonance imaging. Ann Neurol 1997;42:951–962.
12. Pajevic S, Pierpaoli C. Color schemes to represent the orientation of anisotropic tissues from diffusion tensor data: application to white matter fiber tract mapping in the human brain. Magn Reson Med 1999;42:526–540.
13. Wakana S, Jiang H, Nagae-Poetscher LM, van Zijl PC, Mori S. Fiber tract-based atlas of human white matter anatomy. Radiology 2004;230:77–87.
14. Xue R, van Zijl PC, Crain BJ, Solaiyappan M, Mori S. In vivo three-dimensional reconstruction of rat brain axonal projections by diffusion tensor imaging. Magn Reson Med 1999;42:1123–1127.
15. Conturo TE, Lori NF, Cull TS, et al. Tracking neuronal fiber pathways in the living human brain. Proc Natl Acad Sci U S A 1999;96: 10422–10427.
16. Jones DK, Simmons A, Williams SC, Horsfield MA. Non-invasive assessment of axonal fiber connectivity in the human brain via diffusion tensor MRI. Magn Reson Med 1999; 42:37–41.
17. Mukherjee P, Miller JH, Shimony JS, et al. Normal brain maturation during childhood: developmental trends characterized with diffusion-tensor MR imaging. Radiology 2001; 221:349–358.
18. Zhai G, Lin W, Wilber KP, Gerig G, Gilmore JH. Comparisons of regional white matter diffusion in healthy neonates and adults performed with a 3.0-T head-only MR imaging unit. Radiology 2003;229:673–681.
19. Lee SK, Mori S, Kim DJ, Kim SY, Kim SY, Kim DI. Diffusion tensor MR imaging visualizes the altered hemispheric fiber connection in callosal dysgenesis. AJNR Am J Neuroradiol 2004;25:25–28.
20. Glenn OA, Henry RG, Berman JI, et al. DTI-based three-dimensional tractography detects differences in the pyramidal tracts of infants and children with congenital hemiparesis. J Magn Reson Imaging 2003;18:641–648.
21. Cowan F. Outcome after intrapartum asphyxia in term infants. Semin Neonatol 2000;5:127–140.
22. Barnett A, Mercuri E, Rutherford M, et al. Neurological and perceptual-motor outcome at 5–6 years of age in children with neonatal encephalopathy: relationship with neonatal brain MRI. Neuropediatrics 2002;33:242–248.
23. Amiel-Tison C, Maillard F, Lebrun F, et al. Neurological and physical maturation in normal growth singletons from 37 to 41 weeks' gestation. Early Hum Dev 1999;54:145–156.
24. Jones DK, Horsfield MA, Simmons A. Optimal strategies for measuring diffusion in anisotropic systems by magnetic resonance imaging. Magn Reson Med 1999;42:515–525.
25. Vilanova A, Berenschot G, van Pul C. DTI Visualization with stream surfaces and evenly-spaced volume seeding. Eurographics/IEEE TCVG VisSym 2004; 173–182.
26. Jellison BJ, Field AS, Medow J, Lazar M, Salamat MS, Alexander AL. Diffusion tensor imaging of cerebral white matter: a pictorial review of physics, fiber tract anatomy, and tumor imaging patterns. AJNR Am J Neuroradiol 2004;25:356–369.
27. Kier EL, Staib LH, Davis LM, Bronen RA. Anatomic dissection tractography: a new method for precise MR localization of white matter tracts. AJNR Am J Neuroradiol 2004; 25:670–676.

28. Kier EL, Staib LH, Davis LM, Bronen RA. MR imaging of the temporal stem: anatomic dissection tractography of the uncinate fasciculus, inferior occipitofrontal fasciculus, and Meyer's loop of the optic radiation. AJNR Am J Neuroradiol 2004;25:677–691.

29. Bahn MM. Comparison of scalar measures used in magnetic resonance diffusion tensor imaging. J Magn Reson 1999;139:1–7.

30. Talairach J, Tournoux P. Referentially oriented cerebral MRI anatomy. Stuttgart, Germany: Thieme Verlag, 1993.

31. Mori S, Kaufmann WE, Davatzikos C, et al. Imaging cortical association tracts in the human brain using diffusion-tensor-based axonal tracking. Magn Reson Med 2002;47:215–223.

32. Counsell SJ, Maalouf EF, Fletcher AM, et al. MR imaging assessment of myelination in the very preterm brain. AJNR Am J Neuroradiol 2002;23:872–881.

33. Wieshmann UC, Clark CA, Symms MR, Franconi F, Barker GJ, Shorvon SD. Anisotropy of water diffusion in corona radiata and cerebral peduncle in patients with hemiparesis. Neuroimage 1999;10:225–230.

34. van Pul C, Buijs J, Janssen MJ, Roos GF, Vlaardingerbroek MT, Wijn PF. Selecting the best index for following the temporal evolution of apparent diffusion coefficient and diffusion anisotropy after hypoxic-ischemic white matter injury in neonates. AJNR Am J Neuroradiol 2005;26(3):469–481.

35. Scollan DF, Holmes A, Winslow R, Forder J. Histological validation of myocardial microstructure obtained from diffusion tensor magnetic resonance imaging. Am J Physiol 1998;275(6 pt 2):H2308–H2318.

36. Holmes AA, Scollan DF, Winslow RL. Direct histological validation of diffusion tensor MRI in formaldehyde-fixed myocardium. Magn Reson Med 2000;44:157–161.

37. Tseng WY, Wedeen VJ, Reese TG, Smith RN, Halpern EF. Diffusion tensor MRI of myocardial fibers and sheets: correspondence with visible cut-face texture. J Magn Reson Imaging 2003;17:31–42.

38. Douglas C, Montgomery G. Applied statistics and probability for engineers. New York, NY: Wiley, 1999.

39. Basser PJ, Pajevic S, Pierpaoli C, Duda J, Aldroubi A. In vivo fiber tractography using DT-MRI data. Magn Reson Med 2000;44:625–632.

40. Tournier JD, Calamante F, King MD, Gadian DG, Connelly A. Limitations and requirements of diffusion tensor fiber tracking: an assessment using simulations. Magn Reson Med 2002;47:701–708.

View publication stats